means of a capillary pipette brought to the bottom (glued quartz glass) to avoid trapping of air bubbles. The procedure is conveniently performed with the naked eye or under a low-power stereomicroscope. A small amount of excess fluid (~1 µl) above the rim of the cuvet prevents bubbletrapping when the screw is fastened to the socket. The risk of bubble formation is not serious even with detergent-containing media, e.g. SDS 0.5%.

The outer dimensions of the casing conform to the microcellhousing assessories (No. 507425) of the Zeiss PMQ II and PMQ 3 spectrophotometers, but may easily be adjusted for other instruments. The dimensions of the cuvet depicted in Figure 1 give a nominal volume of about 4 µl with an optical pathlength of 5 mm, but these dimensions can be arbitrarily changed by selecting different bored glass-tubings. Cleaning the cuvets is made by flushing the cavity with water by use of a hypodermic syringe.

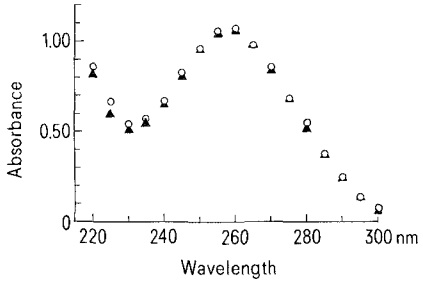

Fig. 2. UV-absorption spectrum of a preparation of rat brain microsomal RNA[5] as determined in a Zeiss quartz MT 2 cuvet (▲) and in the microcuvet described here (O). RNA was dissolved in 0.0036 *M* *Tris*-HCl, pH 7.6; 0.0034 *M* NaH_2PO_4; 0.0001 *M* EDTA; 10% sucrose. 150 and 5 µl of the solution were read respectively. The absorbance values for the microcuvet were corrected for the difference in pathlength by a factor 2.

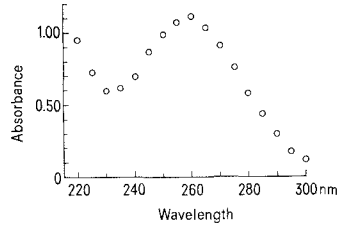

Fig. 3. UV-absorption spectrum of RNA extracted from a sample (about 5 mg) of the CA3 region of rat brain hippocampus as determined in the microcuvet. RNA was extracted according to a micromethod described previously[3] with the addition of a DNase treatment and a final ethanol precipitation. The RNA pellet was dissolved in 10 µl of sample buffer[2], 8 µl of the sample were taken for subsequent electrophoresis and a 2 µl aliquot was taken, diluted to 6 µl with the buffer and read in the microcuvet described.

We tested the accuracy of the measurements in this microcuvet by determining the UV-spectrum of microsomal RNA macroextracted from rat brain[5] both in an ordinary quartz cuvet (Zeiss MT 2) and in the cuvet described. In the first case we used 0.150 ml and in the second 5 µl of sample. The result, reported in Figure 2, shows an almost perfect agreement between the 2 sets of measurements with only slight differences at 220 and 225 nm. Moreover, readings after consecutive refillings indicate a high reproducibility of the measurements (Table).

As an example of application of the microcuvet, we report in Figure 3 the UV-spectrum of RNA extracted from a few milligrams of the CA3 region of rat brain hippocampus by a micro-method described previously[3]. This case is one of those where it would have been impossible to use standard cuvets for UV-absorbance measurements.

A microcuvet in the form of a capillary tube suitable for use in the Zeiss PMQ II microcuvet housing was described previously[6]. We think that the system described here presents two advantages, first the optical properties are accurate within a wider range of optical densities (Figure 1), second the mechanical build-up ensures a tight closure of the cuvet with no risk of bubble formation during prolonged measurements (e.g. determination of reaction kinetics or recording the spectrum of a substance).

The use of our cuvet may easily be extended to the visible range of the spectrum just by blackening its flat ends. An obvious utilization of such an extension appears to be the reduction to the microscale of the colour reactions for RNA, DNA and protein quantitation[7–9].

[5] A. Cupello and H. Hydén, J. Neurochem. *25*, 399 (1975).
[6] D. S. Howell, J. C. Pita and J. F. Marquez, Analyt. Chem. *38*, 434 (1966).
[7] W. C. Schneider, Meth. Enzymol. *3*, 680 (1957).
[8] K. Burton, Meth. Enzymol. *12*, 163 (1957).
[9] O. H. Lowry, N. J. Rosebrough, A. L. Farr and R. J. Randall, J. biol. Chem. *193*, 265 (1951).

Directional Non-Uniformity of Pulsatile Intramyocardial Pressure

T. Koyama, T. Yagi, T. Sasajima and Y. Kakiuchi

Division of Physiology and Division of Ferroelectrics, Research Institute of Applied Electricity, Hokkaido University, 060 Sapporo N-12 W-6 (Japan), 21 June 1976.

Summary. A method using piezoelectric ceramics was newly devised which permitted measurements of intramyocardial pressure. In open-chest dogs, a directional non-uniformity of the intramyocardial pressure was observed, which may be attributable to the variation in the myocardial fibre orientation.

The musculature of the left ventricle consists of muscle layers gradually alter their orientation from the epicardial surface to the subendocardium. Myocardial fibres of each subsectional layer run in a specified direction. Therefore, the regional pulsatile intramyocardial pressure (IMP) caused by fibre contraction may have different force vectors according to the depth from the ventricular surface. To understand the physiological significance of such a non-uniform structure of the left ventricular myocardium, a small sensor was constructed, which permitted the measurement of local pulsatile intramyocardial pressure acting in a specified direction; it was used to measure

anisotropic intramyocardial pressure in the middle and deep portions of the dog's left ventricular wall.

A thin rectangular bar ($2.0 \times 1.0 \times 0.4$ mm in length, width and thickness, respectively) of piezoelectric ceramics, having an electrically conductive coating on the upper and lower surfaces as electrodes for signal sampling, was attached to a thin flexible polyvinyl tube and coated with resin for electrical insulation. This pressure sensor yielded a positive signal in response to a stress acting parallel to the direction of poling, which is referred to as the 3-axis to according conventional technological notation (the pressure voltage output coefficient for this direction, $g_{33} = 38.1 \times 10^{-3}$ V · m/N). The lateral surfaces of this sensor, which were normal to the 3-axis (i.e. the 1-axis), yielded a negative coefficient ($g_{31} = -15.1 \times 10^{-3}$ V · m/N). When the 3- and 1-axis pressure, P_1 and P_2, acted simultaneously on the sensor, as schematically illustrated in Figure 1 A, the output signal became a summation of the positive and negative signals. The voltage amplitude (V_1) of the complex output signal is given by the following equation;

$$V_1 = (g_{33} \cdot P_1 + g_{31} \cdot P_2) \cdot d \quad (1),$$

where d is the thickness of the sensor. When the sensor is rotated by 90 degrees, P_1 and P_2 act on the sensor in the direction of the 1- and 3-axis, respectively (Figure 1 B). Then the voltage amplitude V_2 is given by the following equation;

$$V_2 = (g_{33} \cdot P_2 + g_{31} \cdot P_1) \cdot d \quad (2).$$

When V_1 and V_2 are measured, P_1 and P_2 can be obtained by solving simultaneously equations (1) and (2). In the ventricular myocardium of a beating heart, the pressure will act in various directions simultaneously. The complex pressure can be arbitrarily divided into 3 components of longitudinal, circumferential and radial directions. (The radial component could not be detected by the present pressure sensor.) If one component acts in the direction of the 3-axis, the other acts in the 1-axis and vice versa. In such a situation, the present pressure sensor will act as a kind of convenient rectangular differential pressure detector.

In the experiments using anesthetized dogs, the 3-axis of the sensor was alternately positioned approximetely parallel and nearly perpendicular to the base-apex line of the ventricle as indicated by the arrows in the schematic illustration of the heart, so as to receive longitudinal and circumferential IMP's. The output signals obtained in these positions were denoted as $V_{\parallel}$ and $V_{\perp}$, respectively. Such a positioning was tested at different depths of insertion of the sensor. The centre of the sensitive surface of the sensor was located 8 mm (suffixed deep) or 4 mm (suffixed middle) from the epicardial surface. Thus, the

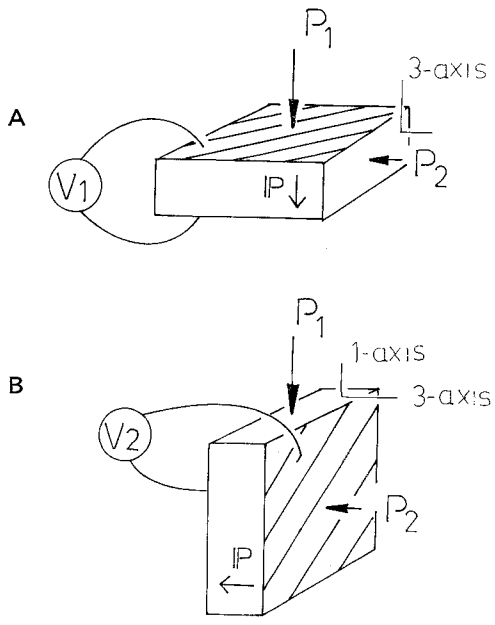

Fig. 1. Geometric relation between pressure, P_1 and P_2, and direction of poling (denoted by IP, i.e. the 3-axis). A) in a position where P_1 acts in a direction of the 3-axis of the ceramic bar. B) after rotation of the ceramic bar by 90 degrees, where P_1 acts in the direction of the 1-axis. Striated surfaces indicate the electrical conductive coating, which act as electrodes for signal sampling.

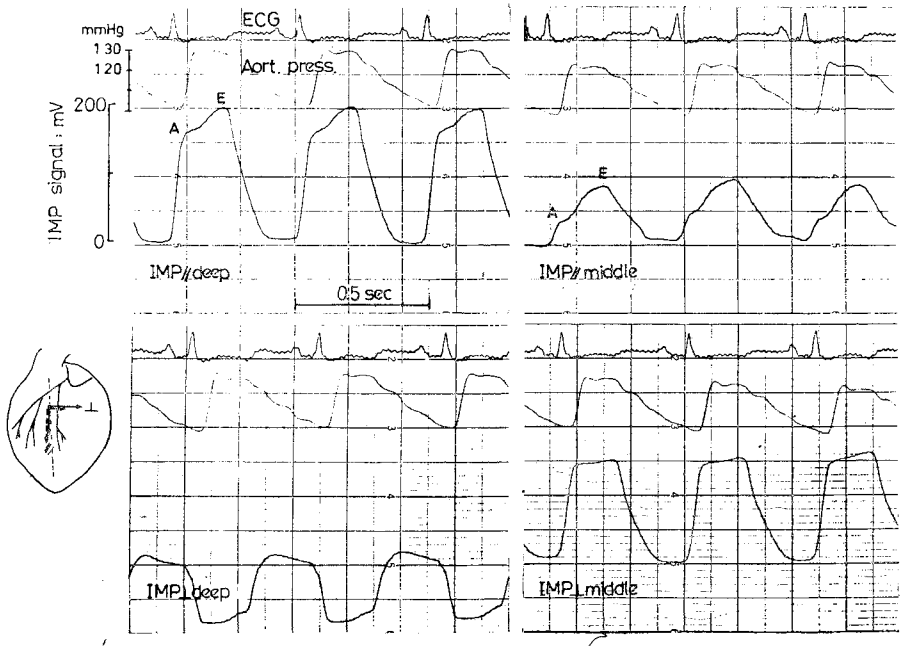

Fig. 2. An example of an actual recording of output signals from the pressure sensor at 4 placements in the myocardium. The curves from top to bottom represent ECG, abdominal aortic pressure and output signal (V's). The dotted line in the schematic illustration of the heart indicates the base-apex line. The broken and straight arrows show directional positions of the 3-axis of the pressure sensor.

signals used for IMP calculations were obtained from 4 placements of the sensitive surface in each serial measurement.

A set of serial recordings obtained by a sensor placed in the myocardium is shown in Figure 2. Each output signal shows a different amplitude and characteristic contour specific for the position of the sensor. The $V_{\parallel}$ deep increases sharply to point A for about 0.08 sec (isovolumetric systole phase) prior to the rise of the aortic curve. Then the increment clearly slows down and comes to a termination at E, a point which coincides with the end of systole on the aortic curve (this period corresponds to ejection phase). In the recording of $V_{\parallel}$ middle, the initial rise to A is small, while the slow rise thereafter is still clear. $V_{\perp}$ middle shows a larger deflection than $V_{\parallel}$ middle and its configuration consists of a sharp rise, followed by a very slow rise which almost forms a plateau during the ejection phase. $V_{\perp}$ deep shows a negative deflection in clear contrast to the curves obtained at the other 3 placements; slightly prior to the aortic rise, the curve begins to fall downwards. IMP's were calculated as P_1 and P_2 of equations (1) and (2) using the peak amplitude of V's. Since the IMP's calculated by the equations represented pressure acting in a direction parallel or perpendicular to the base-apex line, these IMP's were also suffixed by $_{\parallel}$ or $_{\perp}$. The peak amplitudes of V's and calculated IMP's are summarized in the Table. $IMP_{\parallel}$ deep, i.e. longitudinal IMP in the deep portion, was slightly smaller than the systolic aortic pressure and largely exceeded $IMP_{\perp}$ deep, the circumferential IMP in the deep portion. The $IMP_{\perp}$ middle was larger than $IMP_{\parallel}$ middle but did not attain $IMP_{\parallel}$ deep. After measurements, the ventricle was isolated and boiled in a saturated salt solution containing a small amount of detergent for 2 h. The myocaridal fibre of the ventricles could then easily be skinned off, permitting a simple inspection of its direction. The fibre orientation was circumferential in the middle portion and almost parallel to the base-apex line in the deep portion. These observations indicated that the directional non-uniformity of IMP may have been due to the variation in myocardial orientation. These results seem to coincide qualitatively with the results obtained using a strain gauge arch, where different contractile forces were also observed at different positions[1,2]. The ventricle is not a simple thick-walled ellipsoid, but has a fine structure consisting of contractile fibres and densely distributed vascular network. Such a structure may produce the conditions where the summation of the contractile forces becomes a vectoral IMP.

Pulsatile deflections of output signal (V's) and calculated longitudinal and circumferential intramyocardial pressure (IMP's) in the middle and deep portions of the left ventricular myocardium

	Volts			mm Hg		p[a]
	Mean	SD		Mean	SD	
$V_{\parallel}$deep	0.237	0.029	$IMP_{\parallel}$deep	121.0	16.6	
$V_{\parallel}$middle	0.069	0.018	$IMP_{\parallel}$middle	72.6	10.2	<0.01
$V_{\perp}$deep	−0.083	0.031	$IMP_{\perp}$deep	6.4	2.3	<0.01
$V_{\perp}$middle	0.137	0.024	$IMP_{\perp}$middle	97.8	13.9	<0.05

Mean and SD of 7 serial measurements. Abdominal aortic blood pressure was 130/100 mm Hg on the average. [a] Student's t-test, indicating the statistical difference of values as compared to $IMP_{\parallel}$-deep.

[1] E. H. Sonnenblick and E. S. Kirk, Cardiology *56*, 302 (1971/72).
[2] N. W. Robie and W. H. Newman, J. appl. Physiol. *36*, 20 (1974).

A Heated Stage and Tissue Culture Chamber for Electrophysiology

L. Bonkowski and H. I. Runion[1]

University of the Pacific School of Pharmacy, 751 Brookside Road, Stockton (California 95211, USA), 15 April 1976.

Summary. A simple, inexpensive heating circuit is described for use with a warmed microscope stage, small tissue bath, and heated tissue culture chamber. A major consideration in the design of the apparatus is a compatability with electrophysiological studies. Thus, proper shielding and low profile for microelectrode positioning are featured.

This paper describes a heating system which is suitable for use in electrophysiological studies of avian and mammalian tissues in vitro. A warmed microscope stage with tissue bath and a warmed tissue culture chamber are presented. In each device, continuous, controlable heat is provided to a vibration-free, perfusable chamber. There is adequate access to the tissue for microelectrodes, and when grounded, the aluminium warming portions of each device act as an effective Faraday shield to the preparation, reducing the necessity for a separate cage.

Heating circuit. The design of the heating system is simple (Figure 1). A feedback controlled operational amplifier and power transistor form the basis of the proportional heating, temperature control system. Thermistors in a bridge configuration provide the necessary input information to the operational amplifier. One thermistor serves as an ambient temperature sensor (AIR) to detect and create compensation for heat dissapation changes that result from variations in room temperature. The second thermistor (BATH) is encapsulated within the aluminium of the warm stage or culture chamber near the heating element and monitors chamber temperature.

When the device is cold, the high resistance of the BATH thermistor will unbalance the bridge to increase the potential difference across the inputs of the operational amplifier. The transistor (NPN 2N3055) controls the power in the heating circuit. An increased voltage applied to the base will increase the current supplied to the heating element. As the device warms, the resistance of the BATH thermistor will decrease, lowering the potential

[1] Acknowledgment. We wish to thank William F. Dryden for his helpful comments and advice in apparatus design.